ACADEMIC PRESS

Available online at www.sciencedirect.com

SCIENCE DIRECT®

Journal of Sound and Vibration 261 (2003) 839–858

JOURNAL OF SOUND AND VIBRATION

www.elsevier.com/locate/jsvi

Plane wave interpolation in direct collocation boundary element method for radiation and wave scattering: numerical aspects and applications

E. Perrey-Debain*, J. Trevelyan, P. Bettess

Science Laboratories, School of Engineering, University of Durham, South Road, Durham, UK DH1 3LE

Received 2 January 2002; accepted 10 April 2002

Abstract

The classical boundary element formulation for the Helmholtz equation is rehearsed, and its limitations with respect to the number of variables needed to model a wavelength are explained. A new type of interpolation for the potential is then described in which the usual boundary element shape functions are modified by the inclusion of a set of plane waves, propagating in a range of directions. This is termed the plane wave basis boundary element method. The modifications needed to the classical procedures, in terms of integration of the element matrices, and location of collocation points are described. The well-known Singular Value Decomposition solution technique, which is adopted here for the solution of the system matrix equation in its complex form, is briefly outlined. The conditioning of the system matrix is analysed for a simple radiation problem. The corresponding diffraction problem is also analysed and results are compared with analytical and classical boundary element solutions. The CHIEF method is adopted to enhance the quality of the solution, particularly in the vicinity of irregular frequencies. The plane wave basis boundary element method is then applied to two problems: scattering of plane waves by an elliptical cylinder and the multiple circular cylinder plane wave scattering problem. In both cases results are compared with analytical solutions. The results clearly demonstrate that the new method is considerably more efficient than the classical approach. For a given number of degrees of freedom, the frequency for which accurate results can be obtained, using the new technique, can be up to three or four times higher than that of the classical method. This makes the method a powerful new addition to our tools for tackling high-frequency radiation and scattering problems.

*Corresponding author: Tel.: +00-44-191-374-70-94; fax: +1-44-191-374-72-53.
E-mail address: e.g.n.perrey-debain@durham.ac.uk (E. Perrey-Debain).

0022-460X/02/$ - see front matter
PII: S0022-460X(02)01006-4

1. Introduction

Over the last forty or so years, the finite element, boundary element and finite difference numerical methods have been spectacularly successful at solving a wide range of problems in science and engineering. These range from the modelling of geophysical problems through structural and stress analysis, to the prediction of the behaviour of semi-conductor devices, to mention only three important fields, out of dozens. The methods are so well known that no survey of the research papers is necessary. Some flavour of the many finite element applications can be gained from the book by Zienkiewicz and Taylor [1], while boundary element applications have been described by Brebbia [2]. These two techniques are complementary so that, although use of finite elements has always been more widespread, boundary elements remain useful for several classes of engineering problems.

Despite the sweeping success of these computer-based methods, there remain many fields, of great interest, where conventional numerical techniques cannot model the problem in sufficient detail. Examples include materials with microstructure, such as composites, turbulent flows, with much fine detail in microscopic eddies, and, the topic of this paper, very short waves. Very short waves occur in many applications of great scientific and engineering interest. These include, for example, high-frequency acoustics, quantum mechanics, and electro-magnetic wave scattering. All such problems can be modelled satisfactorily using conventional finite element, boundary element, or finite difference methods. The difficulty lies in the requirement that all these methods have about 10 nodal points, per wavelength. (There is a more precise mathematical statement of the modelling requirement, see for example Babuška *et al.* [3,4].) In three dimensions this means that the number of finite element nodes required is at least proportional to 1000 times the number of wavelengths in each spatial direction in the numerical model. For a boundary element model, the 10 node per wavelength requirement is also stipulated, since one is still aiming to capture the essential information in a sinusoidally varying waveform. However, the number of nodes varies in two dimensions only, leading to a quantity given by at least 100 times the number of wavelengths in each surface direction.

Take a specific example. Consider an aeroplane which is scattering radar waves of frequency 30 GHz. The wavelength is seen to be $\lambda = 10^{-2}$ m. For simplicity, take the scattering object to be a sphere of radius $r = 10$ m. Then the surface area of the sphere is approximately $1200\,\mathrm{m}^2$, or 12×10^6 square wavelengths. With 10 nodes per wavelength, this leads to the need for 1.2×10^9 nodal variables. The classical boundary element matrix would thus contain 1.44×10^{18} terms. It is evident that even with the most powerful computers available now, or in the foreseeable future, such problems are not soluble.

To make any progress, it is necessary to use a better model of the waves, which will describe them using fewer parameters. One approach for doing this, the subject of this paper, is to include some knowledge of the waves in the element formulation. This was first done for infinite elements by Bettess and Zienkiewicz [5,6], and the concept has been further developed [7]. The idea of including the wave shape in a finite element was first adopted by Astley [8–10], who has also contributed a recent survey of developments in infinite elements [11]. These ideas were further developed by Chadwick *et al.* [12]. The above concepts were developed in an *ad hoc* manner for specific wave problems. The next key step was by Melenk and Babuška, who included multiple wave directions in finite elements for short wave problems [13,14]. The concept was formulated

under the general heading of "Partition of Unity Finite Elements Method" (PUFEM), which is a broadly applicable concept which can be used for other situations in which microstructure is present [15]. In simple terms the basic idea is that the presence of conventional finite element polynomials ensures convergence as the mesh is refined, while additional functions (in our case plane waves), enrich the solution space and allow accurate solutions with a coarse mesh. This idea has been further extended by Laghrouche and Bettess [16–18], Ortiz and Sanchez [19], Mayer and Mendel [20] and Farhat *et al.* [21]. Essentially, instead of using the conventional finite element approximation within each element, a set of plane waves is also included. Although this introduces extra variables, it means that it is no longer necessary to have 10 nodes per wavelength, and indeed there can be many wavelengths between nodes. Thus a modelling process which could be applicable to extremely short waves has been achieved.

From the earliest days of the development of boundary elements, it has been recognised that there is a commonality of method with finite elements, in the representation of the unknown function. Indeed the identical "shape function" interpolations are often adopted. It is therefore very natural to ask whether the ideas described above, which have worked in finite elements, can also succeed with boundary elements. In previous years, the same idea has been theoretically investigated by de La Bourdonnaye [22,23] under the title of Microlocal Discretization for solving scattering problems with integral equations. Its results strongly support the use of the plane wave approximation, especially at high frequency, though no numerical results were reported.

This paper will show that this new finite element basis can be applied in a boundary element formulation and that the accuracies and economies over conventional wave modelling techniques are very substantial. A brief preliminary note [24] described the outlines of the method. In this paper all the details of the implementation of the method, and the investigation of its accuracy and numerical characteristics, including the condition number of the resulting boundary element matrices are given. The new method, which the authors believe will have a significant impact on the modelling of short wave problems in many different fields, is also applied to a range of sample problems. The conjecture that the method is orthogonal to the increasingly popular Fast Multipole Method [25] or other fast iterative solver method [26] remains to be explored and it is hoped that the benefits of the two approaches will be additive.

2. Mathematical formulation

2.1. Helmholtz integral equations

Let Ω be a two-dimensional obstacle of smooth boundary line Γ in an infinite propagative medium. Throughout this paper, active or passive obstacles with constant complex-valued admittance v and radiating source v will be considered. The mathematical treatment of the scattering of an incident time-harmonic wave ϕ^I by Ω leads to the surface Helmholtz integral representation formula for the unknown potential ϕ ($e^{-i\omega t}$ time-dependence)

$$\tfrac{1}{2}\phi(x) + (\mathscr{K}\phi)(x) - v(\mathscr{S}\phi)(x) = \phi^I(x) + (\mathscr{S}v)(x), \quad x \in \Gamma, \tag{1}$$

where

$$(\mathscr{S}\phi)(x) = \int_\Gamma G(x,y)\phi(y)\,\mathrm{d}\Gamma_y \quad \text{and} \quad (\mathscr{K}\phi)(x) = \int_\Gamma \frac{\partial G(x,y)}{\partial n}\phi(y)\,\mathrm{d}\Gamma_y \tag{2}$$

denote the single and double-layer potentials. Here, $G(x,y) = \mathrm{i}/4\,\mathrm{H}_0(k|x-y|)$ is the free-space Green function with wavenumber k and n is the inward normal unit vector. H_0 denotes the Hankel function of the first kind of zero order and $\mathrm{i} = \sqrt{-1}$. For a brief nomenclature $v = 0$ corresponds to a hard boundary condition and $|v| = \infty$ will be referred to as a soft boundary condition.

Even though the Helmholtz problem in the exterior domain has a unique solution, the boundary formulation (1) is known to be singular when k is an eigenfrequency of a corresponding interior problem. This non-uniqueness problem is numerically manifested in a one rank deficiency of the system matrix and leads to ill-conditioned systems in a range of frequencies whose bandwidth is strongly related to the quality of the approximation and the mesh discretization [27]. Various alternative formulations of this exterior problem have been suggested to eliminate these difficulties (see for instance Ref. [28]). Among them, the Combined Helmholtz Integral Equation Formulation (CHIEF) proposed by Schenck [29] has the advantage of being easier to implement and computationally less expensive than the other alternative methods. This formulation uses the interior Helmholtz integral equation with points $x^c_{i=1..N_c}$ called CHIEF points inside the body as a constraint to form an overdetermined system of equations

$$(\mathscr{K}\phi)(x_i^c) - v(\mathscr{S}\phi)(x_i^c) = \phi^I(x_i^c) + (\mathscr{S}v)(x_i^c), \quad x_i^c \in \Omega. \tag{3}$$

This formulation has the drawback that points falling on any nodal surface of the related interior problem do not provide linearly independent constraints. However, it will be assumed in the sequel that these unfortunate situations are not being faced, though note that such situations are normally avoided by using multiple CHIEF points.

2.2. Finite element basis

A mathematical justification for the use of the plane wave approximation in the integral equation (1) is beyond the scope of this paper. The reader will find some elements of an answer regarding the finite element method from the work of Melenk and Babuška, in which the main results concerning the Helmholtz equation can be found in Section 3.3 in Ref. [13]. The second approach developed by de La Bourdonnaye [22,23] finds its justification in geometrical optics. The author assumes that the solution of the integral equation can be written as a sum of terms like $a(x,k)\mathrm{e}^{\mathrm{i}k\psi(x)}$ where $a(x,k)$ admits a development in $1/k$. For k sufficiently large, the gradient of the phase ψ is of unit amplitude due to the eikonal equation. Therefore, locally, the solution is asymptotically equivalent to a finite sum of terms like $a(x)\mathrm{e}^{\mathrm{i}k\xi\cdot x}$ with $|\xi| = 1$. This form is very similar to the system of plane waves introduced in Ref. [13]. It suggests that one should take $a_i(x)\mathrm{e}^{\mathrm{i}k\xi_i\cdot x}$ as basis functions, where the functions a_i are compactly supported on Γ and the vectors ξ_i describe the unit circle. In this paper, these functions have been chosen to be the standard

quadratic shape functions associated with the partition of the boundary

$$\Gamma = \bigcup_{n=1}^{N} \Gamma_n,$$

where Γ_n is analytic and given through $\Gamma_n = \{\gamma_n(\eta): -1 \leqslant \eta \leqslant 1\}$. On each element, the potential is then approximated as

$$\phi(x) = \sum_{p=1}^{3} \sum_{l=1}^{M} a_{p,l}^{n}(x)\phi_{p,l}^{n}, \tag{4}$$

where the finite element basis $a_{p,l}^{n}$ is the product of the quadratic Lagrangian polynomial N_p with a plane wave of direction ξ_l, namely

$$a_{p,l}^{n}(x(\eta)) = N_p(\eta)\mathrm{e}^{\mathrm{i}k\xi_l \cdot x}. \tag{5}$$

The continuity of ϕ between two adjacent elements will be satisfied if

$$\phi_{3,l}^{n-1} = \phi_{1,l}^{n} \quad \text{for } (n,l) \in [1,N] \times [1,M], \tag{6}$$

where the index 0 is assimilated with index N. Now, in order to give a simple representation of ϕ on the boundary Γ, it is convenient to group the set of indices (n,p,l) into a single index. To do this, let g be a one-to-one mapping from the set of indices $(n,p,l) \in [1,N] \times [1,2] \times [1,M]$ to the single index $j \in [1,N_d]$ where $N_d = 2NM$ is the total number of degrees of freedom. The potential on Γ can be formally written as

$$\phi(x) = \sum_{j=1}^{N_d} q_j(x)\phi_j = \mathbf{q}^{\mathrm{T}}(x)\boldsymbol{\phi}, \tag{7}$$

where the functions q_j are defined as follows:

$$q_j = a_{1,l}^{n} + a_{3,l}^{n-1}, \quad j = g(n,1,l), \tag{8}$$

$$q_j = a_{2,l}^{n}, \quad j = g(n,2,l), \tag{9}$$

and $\phi_{p,l}^{n}$ has been replaced by $\phi_{j=g(n,p,l)}$. Though there is no restriction concerning the directions ξ_l, these are taken to be evenly distributed on the unit circle,

$$\xi_l = (\cos\alpha_l, \sin\alpha_l) \quad \text{with } \alpha_l = 2\pi l/M.$$

Employing an engineering terminology, the element Γ_n and the associated approximation (4) will be referred to as a wave boundary element. Let us finish this section by mentioning that the plane wave approximation (4) automatically contains the conventional quadratic interpolation by simply setting $M = 1$ and $\xi_1 = 0$. This feature will allow a fair comparison between the usual polynomial interpolation and the new plane wave basis whatever the geometry of the curve Γ.

2.3. Element matrices and numerical integration

When using conventional boundary elements, the collocation points are the natural nodes of the finite element mesh. The new type of approximation (3) requires the definition of some extra collocation points in order to produce a square system. These points have been chosen arbitrarily

to be distributed along each element Γ_n as

$$x_{i=g(n,p,l)} = \left\{\gamma_n(\eta_{p,l}):\eta_{p,l} = p - 2 + (l-1)/M\right\}. \tag{10}$$

The case $M = 1$ corresponds to the natural nodes of the quadratic interpolation. One can note that the collocation points as defined above will be regularly distributed in the real space whenever Γ_n is a portion of either a straight line or a circle. In other cases, the distortion between parametric space and real space will have to be considered. The matrix system is obtained by applying Eq. (1) at the collocation points giving

$$\mathbf{A}\boldsymbol{\phi} = \left(\frac{\mathbf{W}}{2} + \mathbf{K} - v\mathbf{S}\right)\boldsymbol{\phi} = \mathbf{b}, \tag{11}$$

where $W_{ij} = q_j(x_i)$ denotes the interpolation matrix ($W_{ij} = \delta_{ij}$ when $M = 1$), $K_{ij} = (\mathscr{K}q_j)(x_i)$ and $S_{ij} = (\mathscr{S}q_j)(x_i)$ are the boundary element matrices and $b_i = \phi^I(x_i) + (\mathscr{S}v)(x_i)$ is the source vector. The logarithmic singularity of the single-layer potential can be efficiently handled by using the cubic Telles' transformation [30]. Let $f = Gq_j|\mathrm{d}\gamma_n/\mathrm{d}\eta|$ be the singular integrand in the parametric space and $\bar{\eta}$ the local co-ordinate of the singularity. Then

$$\int_{-1}^{1} f(\eta)\,\mathrm{d}\eta = \int_{-1}^{1} f\{[(\gamma-\bar{\gamma})^3 + \bar{\gamma}(\bar{\gamma}^2+3)]/(1+3\bar{\gamma}^2)\}3(\gamma-\bar{\gamma}^2)/(1+3\bar{\gamma}^2)d\gamma,$$

where $\bar{\gamma}$ is the image of $\bar{\eta}$ by the cubic mapping. This non-linear transformation automatically provides a great concentration of points near the singularity and has been shown to be much more efficient than the logarithmic Gaussian quadrature formula. In traditional BEM, the rule of thumb of 4–5 quadratic elements per wavelength with a four-point Gauss–Legendre formula is usually adopted for results of reasonable accuracy [31]. However, the finite element basis (5) allows a significantly increased element size as each element can contain many wavelengths. Therefore, one needs an integration procedure to produce element matrices at any desired accuracy whatever the element length. Here, this is simply done by considering a regular subdivision of the interval $[-1,+1]$ and using 10 Gauss points over each subdivision. Care was taken to ensure that Gauss points did not fall in the close vicinity of a collocation point in order to avoid inaccurate numerical evaluations of the integrands. All operations are performed with double precision and the Green function and its normal derivative are evaluated using the routines for Bessel functions of fractional order (as recommended) from Ref. [32].

2.4. Singular value decomposition

In handling poorly conditioned or overdetermined systems, singular value decomposition (SVD) is often considered the ultimate tool. In the following discussion, situations where the SVD of $\mathbf{A}$ is not affected by the non-uniqueness problem will be considered. This can be done by either considering k far enough from the irregular frequencies or by simply properly choosing some CHIEF points. Non-uniqueness effects have been widely studied in the literature (see for instance Refs. [27,28]) and they will not be discussed here.

The SVD of the complex rectangular $(N_c + N_d) \times N_d$ matrix $\mathbf{A}$ is defined as

$$\mathbf{A} = \mathbf{U}\boldsymbol{\Sigma}\mathbf{V}^{\mathrm{H}}, \tag{12}$$

where $\mathbf{V}^{\mathrm{H}}$ denotes the conjugate transpose of the matrix $\mathbf{V}$. $\mathbf{U}$ and $\mathbf{V}$ are both unitary matrices and $\mathbf{\Sigma}$ is a diagonal matrix with N_d positive or zero elements called the singular values. Without loss of generality the columns of these matrices are assumed to be arranged in order of descending singular values so that $\sigma_1 \geqslant \sigma_2 \geqslant \cdots \geqslant \sigma_{N_d} \geqslant 0$. Assuming that the matrix $\mathbf{A}$ has full rank (i.e., $\sigma_{N_d} \neq 0$), the condition number of the rectangular (or possibly square) matrix $\mathbf{A}$ in the 2-norm is obtained by $\kappa = \sigma_1/\sigma_{N_d}$. Now, let the vectors $\mathbf{V}_i$, $i = 1, \ldots, N_d$ denote the columns of $\mathbf{V}$. Then the solution of (11) can be written as

$$\boldsymbol{\phi} = \sum_{i=1}^{N_d} \frac{\beta_i}{\sigma_i} \mathbf{V}_i, \tag{13}$$

where $\boldsymbol{\beta} = \mathbf{U}^{\mathrm{H}}\mathbf{b}$. The columns in $\mathbf{V}$ can be regarded as an orthogonal basis for the solution space of $\mathbf{A}$, the columns in $\mathbf{U}$ as an orthogonal basis for the range of $\mathbf{A}$ and the β_i's are the coefficients of the right-hand side $\mathbf{b}$ in this basis. When the system is overdetermined ($N_c \neq 0$) then solution (13) is the vector of smallest length minimizing the residual $\|\mathbf{A}\boldsymbol{\phi} - \mathbf{b}\|_2$. To cope with finite precision and inaccuracies of the element matrices, denote the computed version of the quantity $\mathbf{X}$ by $\hat{\mathbf{X}} = \mathbf{X} + \Delta\mathbf{X}$. The SVD algorithm then produces $\hat{\mathbf{A}} = \hat{\mathbf{U}}\hat{\mathbf{\Sigma}}\hat{\mathbf{V}}^{\mathrm{H}}$ with $\hat{\mathbf{\Sigma}} = \mathrm{diag}(\hat{\sigma}_1, \ldots, \hat{\sigma}_{N_d})$ and $\hat{\kappa} = \hat{\sigma}_1/\hat{\sigma}_{N_d}$.

When some of the singular values are very small but non-zero then the matrix $\hat{\mathbf{A}}$ is nearly rank-deficient and the direct application of the computed version of (13) may give rise to poor solutions corrupted by roundoff errors (see Refs. [32,33] for useful discussion on that topic). The deviation $\Delta\mathbf{A}$ is due to the integration procedure and the SVD algorithm itself and the level of accuracy of the approximate matrix $\hat{\mathbf{A}}$ is of order ε, i.e., $\|\Delta\mathbf{A}\|_2 \leqslant \varepsilon\|\mathbf{A}\|_2$. Now, let $\delta > 0$ be a small number and adopt the convention that $\hat{\mathbf{A}}$ has numerical rank $\hat{r}$ if the $\hat{\sigma}_i$ satisfy

$$\hat{\sigma}_1 \geqslant \cdots \geqslant \hat{\sigma}_{\hat{r}} > (\delta\hat{\sigma}_1) \geqslant \hat{\sigma}_{\hat{r}+1} \cdots \geqslant \hat{\sigma}_{N_d}. \tag{14}$$

In other words, one is assuming that $\hat{\mathbf{A}}$ can be fairly approximated by the $\hat{r}$-rank matrix

$$\hat{\mathbf{A}}_{\hat{r}} = \hat{\mathbf{U}}\,\mathrm{diag}(\hat{\sigma}_1, \ldots, \hat{\sigma}_{\hat{r}}, 0, \ldots, 0)\,\hat{\mathbf{V}}^{\mathrm{H}}. \tag{15}$$

By assuming that the 2-norm of the matrices $\Delta\mathbf{U}$ and $\Delta\mathbf{V}^{\mathrm{H}}$ is bounded by ε and given the fact that $\|\mathbf{U}\|_2 = \|\mathbf{V}^{\mathrm{H}}\|_2 = 1$, gives the following inequality:

$$\|\hat{\mathbf{U}}\,\mathrm{diag}(0, \ldots, 0, \hat{\sigma}_{\hat{r}+1}, \ldots, \hat{\sigma}_{N_d})\,\hat{\mathbf{V}}^{\mathrm{H}}\|_2 \leqslant \hat{\sigma}_{\hat{r}+1}\ (1 + 2\varepsilon + \varepsilon^2). \tag{16}$$

Thus, for ε sufficiently small, the 2-norm of the ignored part of $\hat{\mathbf{A}}$ is bounded by $\delta\hat{\sigma}_1 \approx \delta\|\mathbf{A}\|_2$. Therefore, the singular values whose magnitude are below ε are likely to reflect "noise" rather than significant information. Then, by choosing $\delta < \varepsilon$, one can expect the truncated vector solution

$$\hat{\boldsymbol{\phi}}_{\hat{r}} = \sum_{i=1}^{\hat{r}} \frac{\hat{\beta}_i}{\hat{\sigma}_i} \hat{\mathbf{V}}_i \tag{17}$$

to be a good approximation to $\boldsymbol{\phi}$ provided that the discarded components $\hat{\beta}_i$ ($i > \hat{r}$) are negligible. In other words, the truncation will be effective and reliable on condition that the right-hand side vector $\hat{\mathbf{b}}$ 'almost' lies in the range of $\hat{\mathbf{A}}_{\hat{r}}$. Otherwise, it is likely to cause unacceptable incompatibility. A numerical study carried out in Section 3.2 for a very simple configuration will provide a numerical answer to these issues.

3. Numerical aspects

3.1. Conditioning

It is known from previous work that the new finite element basis (4) gives rise to numerical instabilities manifested in highly ill-conditioned matrices [18,21]. It has been observed that the condition number grows very fast as the number of plane waves becomes large or as the frequency decreases. The analysis of the conditioning is of course related to the formulation, FEM or BEM for instance, and the resolution scheme such as the variational approach or the collocation technique. In the present case, it will be shown that the condition number is mainly governed by only two parameters: the number of collocation points or samples per wavelength, α, and the number M of directions in the plane wave basis. This can be easily demonstrated by observing that expansion (4) shares some similarities with a truncated 1-D Fourier series, the latter being a very particular case of the former.

Consider the ideal case of a single constant element (i.e., $N_1 = 1$ and $N_2 = N_3 = 0$) lying on the real line $x = (s, 0)$. On this element, the approximation has the simple form:

$$\phi(s,0) = \sum_{j=1}^{M} \phi_j e^{ik\xi'_j s}, \quad |\xi'_j| \leqslant 1, \tag{18}$$

where ξ'_j can be interpreted as the projection of the vector ξ_j on the horizontal axis. By considering a regular distribution of coefficients $\{\xi'_j = 2j/M - 1, j = 1, \ldots, M\}$, the previous series is periodic and the interpolation problem can be written as

$$\sum_{j=1}^{M} \phi_j z_i^j = z_i^{M/2} \phi(s_i, 0), \quad z_i = e^{ik(2/M)s_i} \tag{19}$$

where the s_i's are real-valued samples. This is a polynomial interpolation problem that has a unique solution if the nodes z_i, located on the unit circle, are distinct. If the samples are regularly distributed with sampling rate Δ then the interpolation matrix reads

$$W_{ij} = e^{i2\pi(2/\alpha)\,(i\cdot j/M)} \tag{20}$$

in which

$$\alpha = \frac{2\pi}{k\Delta} \tag{21}$$

defines the number of degrees of freedom per wavelength. The conditioning of the interpolation matrix $\mathbf{W}$ is displayed in Table 1. As the number of plane waves M increases, the condition number $\hat{\kappa}$ grows very rapidly with respect to α. Above a certain threshold estimated at 10^{16}, the computer fails in evaluating correctly the condition number (and more precisely the smallest singular values) because the machine precision is reached. An inspection of the SVD of $\mathbf{W}$ reveals that the set of singular values does not split into subsets of small and large singular values. This makes the determination of the numerical rank rather arbitrary. Now observe the particular but positive effect when $\alpha = 2$. For this value, $\mathbf{W}$ exactly corresponds to a Discrete Fourier Transform matrix and $M^{-1/2}\mathbf{W}$ is a unitary transformation, therefore $\kappa = 1$ whatever the system dimension. For higher values ($\alpha > 2$), the condition numbers grow more or less rapidly according to the

number of directions M. However, the nodes z_i are distinct and, despite the very bad conditioning of the interpolation matrix, the system always remains non-singular. When $\alpha<2$, the system is singular if $|\xi'_j - \xi'_{j'}|_{j\neq j'}$ is a multiple of α.

As a test case for comparison with previous results, choose the hard circular cylinder of radius a. The boundary discretization is considered to be perfectly regular and

$$\Gamma_n = \left\{ x(\theta) = a(\cos\theta, \sin\theta) : \frac{2\pi}{N}(n-1) \leqslant \theta \leqslant \frac{2\pi}{N} n \right\}. \tag{22}$$

This allows the following equality:

$$N_d = 2NM = \alpha\, ka$$

to be always satisfied even for the extreme value $M = 1$ corresponding to the conventional approach. It is essential for short wave scattering problems, solved by whatever method, that the geometry of the scatterer be defined precisely as in (22). This matter is discussed in the conclusions.

The condition numbers of the system matrix $\mathbf{A}$ are shown in Table 2 for the particular frequency $ka = 64$. Since the non-uniqueness problem occurs when ka are the zeros of the integer order Bessel functions [28] the closest singular frequency appears at $ka = 64.0629\ldots$. However, its influence on the conditioning is negligible as shown in the first row corresponding to the quadratic approximation. The behaviour with respect to α and M is comparable with Table 1 and small values for α (say $2 \leqslant \alpha \leqslant 3$) produce moderate condition numbers. Here again, values of $\hat{\kappa}$ above 10^{16} are subject to doubt and real values are probably much bigger. In the next two section an error analysis is carried out for two Neumann-like problems associated with the same system matrix of Table 2.

Table 1
Condition numbers for a simple model ($\log_{10}(\hat{\kappa})$)

	$\alpha = 2$	$\alpha = 3$	$\alpha = 4$	$\alpha = 5$	$\alpha = 6$
$M = 8$	0.0	1.9	3.0	3.8	4.5
$M = 16$	0.0	4.5	6.9	8.6	9.9
$M = 32$	0.0	9.9	14.9	16.5	16.3

Table 2
Condition numbers for the hard circular cylinder at $ka = 64$ ($\log_{10}(\hat{\kappa})$)

	$\alpha = 2$	$\alpha = 3$	$\alpha = 4$	$\alpha = 5$	$\alpha = 6$
Quadratic	1.2	1.2	1.2	1.2	1.2
$M = 8$	4.4	5.2 (a)	7.2	8.6	10.3
$M = 16$	3.5	7.5	10.7 (b)	15.1	16.8
$M = 32$	3.9	9.2	16.3 (c)	16.1 (d)	16.9 (e)

3.2. Error analysis for a radiation problem

As a first test case, consider a radiation problem with $v = 1$, $v = 0$ and $ka = 64$. The analytical solution is independent of θ and is given by $\tilde{\phi}|_\Gamma = \mathrm{H}_0(ka)/(k\mathrm{H}_1(ka))$, where H_1 is the Hankel function of the first kind of order one. Because some numerical instabilities are expected especially for highly ill-conditioned system matrices, solution vectors $\hat{\mathbf{V}}_i$ associated with 'small' singular values (i.e., below $\delta\hat{\sigma}_1$) are discarded. Through various numerical experiments, it has been observed that best results were obtained when $10^{-12} \leqslant \delta \leqslant 10^{-13}$. These values are in agreement with Ref. [32] and roughly correspond to the SVD solver accuracy in double precision. The effect of thresholding is displayed in Table 3 for five different cases referenced in Table 2. The L_2 relative error is defined as

$$E_2 = \frac{\|\phi - \tilde{\phi}\|_{L_2(\Gamma)}}{\|\tilde{\phi}\|_{L_2(\Gamma)}}, \tag{23}$$

where ϕ and $\tilde{\phi}$ denote the computed and exact solutions respectively. These values were computed by adding to the system 10 CHIEF constraints in order to cancel any irregular frequency effect on the quality of the solution. For the first two cases, the condition number is too low and the thresholding is not active. An interesting result is the ability of the plane wave basis to represent a constant profile with 6–7 exact digits by using only 4 degrees of freedom per wavelength (case (b)). In situations where the systems are very poorly conditioned (cases (c)–(e)), a cut-off at $\delta = 10^{-12}$ improves the results by 1–3 digits. Note that the accuracy does not improve as drastically as from case (a) to (b). In fact, some missing information is contained in the last discarded vectors $\hat{\mathbf{V}}_i$ and better results would certainly be achieved in a multiple precision context.

Table 4 gives a better understanding of thresholding effects. The first two columns show the Root Mean Square of the truncated solution vector $\hat{\boldsymbol{\phi}}_{\hat{r}}$ and the full one $\hat{\boldsymbol{\phi}}$. Effects on compatibility are illustrated in the next two columns where values for the 2-norm of the residual vectors $\hat{\mathbf{r}}_{\hat{r}} = \hat{\mathbf{A}}\hat{\boldsymbol{\phi}}_{\hat{r}} - \hat{\mathbf{b}}$ and $\hat{\mathbf{r}} = \hat{\mathbf{A}}\hat{\boldsymbol{\phi}} - \hat{\mathbf{b}}$ are shown. The last column gives the magnitude of the discarded components $\hat{\beta}_i$. Though numerical instabilities associated with small singular values strongly perturb the vector solution $\hat{\boldsymbol{\phi}}$, their effects on the L_2 error are rather mild and the good solutions for ϕ recovered after recombination in Eq. (7) can still be obtained even without thresholding. This is mainly due to the fact that the decomposition of the source vector in the $\hat{\mathbf{U}}_i$ basis has very small component $\hat{\beta}_i$ for $i > \hat{r}$ and the numerical rank estimation at $\delta = 10^{-12}$ does not produce a substantial departure from compatibility.

Table 3
Effect of thresholding ($\delta = 10^{-12}$) on the L_2 relative error

	Thresholding (%)	No thresholding (%)
Case (a)	1.45	1.45
Case (b)	9.5×10^{-5}	9.5×10^{-5}
Case (c)	2.2×10^{-6}	1.0×10^{-4}
Case (d)	2.6×10^{-7}	5.0×10^{-3}
Case (e)	2.5×10^{-7}	5.0×10^{-4}

Table 4
Effect of thresholding ($\delta = 10^{-12}$) on the solution vector and the residual

	$N_d^{-1/2}\|\|\hat{\boldsymbol{\phi}}_{\hat{r}}\|\|_2$	$N_d^{-1/2}\|\|\hat{\boldsymbol{\phi}}\|\|_2$	$\|\|\hat{\mathbf{r}}_{\hat{r}}\|\|_2$	$\|\|\hat{\mathbf{r}}\|\|_2$	$\max_{i>\hat{r}}\|\hat{\beta}_i\|$
Case (a)	4.2×10^{-2}	4.2×10^{-2}	1.0×10^{-4}	1.0×10^{-4}	0.0
Case (b)	7.1×10^{-2}	7.1×10^{-2}	1.0×10^{-10}	1.0×10^{-10}	0.0
Case (c)	8.7×10^{-3}	3.6×10^{0}	5.0×10^{-12}	4.0×10^{-12}	1.5×10^{-12}
Case (d)	5.3×10^{-3}	5.9×10^{2}	2.2×10^{-11}	7.2×10^{-11}	9.2×10^{-12}
Case (e)	2.7×10^{-3}	9.2×10^{2}	3.6×10^{-11}	1.3×10^{-10}	2.0×10^{-11}

3.3. Error analysis for a scattering problem

In this section, some results for the scattering of an incident plane wave $\phi^I(x) = \mathrm{e}^{\mathrm{i}kd\cdot x}$ propagating along the horizontal direction $d = (1, 0)$ by a hard circular cylinder of radius a will be presented. In polar co-ordinates, the field can be represented by separable solutions and the exact scattered potential is given by the infinite series [34]:

$$\tilde{\phi}^S(x) = -\frac{\mathrm{J}_0'(ka)}{\mathrm{H}_0'(ka)}\mathrm{H}_0(kr) - 2\sum_{n=1}^{\infty} \mathrm{i}^n \frac{\mathrm{J}_n'(ka)}{\mathrm{H}_n'(ka)}\mathrm{H}_n(kr)\cos n\theta, \tag{24}$$

where $x = r\ (\cos\theta, \sin\theta)$, $\mathrm{H}_n(kr)$ and $\mathrm{J}_n(kr)$ are, respectively, Hankel and Bessel functions of the first kind and order n, and the prime denotes differentiation with respect to kr. This series is well-behaved and allows one to produce very accurate results without deterioration at high frequency. Fig. 1 shows the L_2 relative error corresponding to the same matrix systems as those referenced in Table 2. In all cases, 10 CHIEF equations are used and computed solutions are filtered at $\delta = 10^{-12}$. This exhibits an algebraic-like convergence whose rate depends on the number of directions M. The last two results for the case $M = 32$ are not as good as expected and it is believed that better results would have been achieved in a multiple precision context. One can note that errors obtained are of the same magnitude as those reported in Table 3 concerning the radiation problem. The same experiment has been led without thresholding and effects on the errors are similar to the previous section. Results from the conventional approach are also shown in order to compare the two approaches. The striking result is that for $\alpha \geqslant 3$, the plane wave approximation exhibit errors between *4 and 8 orders of magnitude* smaller than those of the conventional approximation.

In Table 5 are displayed errors obtained with $M = 32$ and $\alpha = 2.5$ for a large frequency range. The associated condition numbers are also presented. The last column shows results obtained by using the quadratic approximation with $\alpha = 10$. In all cases, we used 30 CHIEF equations and $\delta = 10^{-12}$. At low frequency (say $ka < 50$), 2.5 degrees of freedom per wavelength seems too low to obtain a satisfying solution. Results are much more accurate at higher frequencies and this is in agreement with de La Bourdonnaye [23]. Clearly, the accuracies and economies over conventional approximation are very substantial for this frequency range. Because α and M are kept fixed, the condition number grows moderately with respect to the system dimension and the thresholding is not active here.

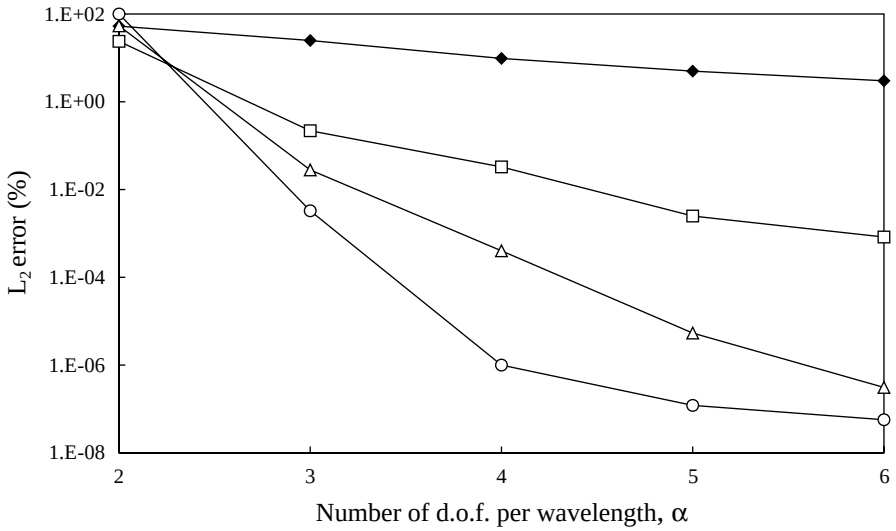

Fig. 1. Error analysis for the hard circular cylinder, $ka = 64$. —□—, $M = 8$; —△—, $M = 16$; —○—, $M = 32$; —◆—, quadratic.

Table 5
Relative L_2 errors for a scattering problem

ka	Rel. L_2 err. (%) $M = 32$, $\alpha = 2.5$	C.N. ($\log_{10}(\hat{\kappa})$) $M = 32$, $\alpha = 2.5$	Rel. L_2 err. (%) Quad., $\alpha = 10$
25.6	11.7	4.1	0.68
51.2	1.68	4.2	0.65
76.8	0.47	4.6	0.74
102.4	0.02	5.3	0.65
128.0	0.05	5.6	0.65
153.6	0.05	5.9	0.65
179.2	0.05	6.0	1.09
256.0	0.02	6.5	Not available
384.0	0.14	7.1	Not available
512.0	0.68	8.0	Not available

In Fig. 2 are displayed the real part of the computed solutions for the two cases $ka = 128$ and 256 along the first wave boundary element Γ_1 located in the shadow zone. It can be checked that both wave elements contains approximately $2M/\alpha \approx 26$ oscillations.

4. Numerical examples

It will be shown that these new wave boundary elements can be used for dealing with a great variety of situations with flat geometries or in the presence of multiple reflections. All numerical

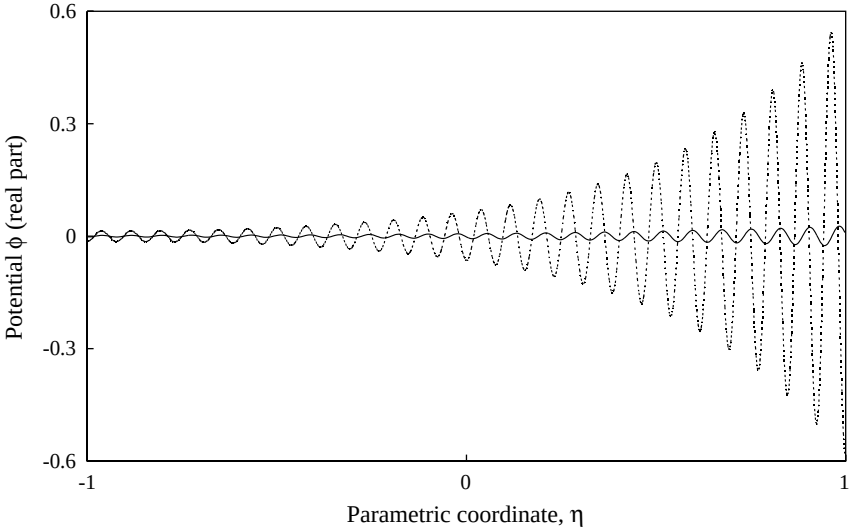

Fig. 2. Potential along a single wave element in the shadow zone. Dashed line, $ka = 128$; straight line, $ka = 256$.

experiments have been performed by using 10 CHIEF equations and solutions are filtered at $\delta = 10^{-12}$.

4.1. Scattering by an elliptical cylinder

Consider the scattering of an incident plane wave propagating along the direction $d = (\cos\theta^I, \sin\theta^I)$ by an elliptical cylinder of semi-major axis a (resp. semi-minor axis b). The analytical solution for the scattered field can be developed in terms of Mathieu functions and is given in Ref. [34]

$$\tilde{\phi}^S(x) = -2\sum_{n=0}^{\infty} \mathrm{i}^n b_n \,\mathrm{ce}_n(\theta^I, h)\mathrm{ce}_n(\theta, h) - 2\sum_{n=1}^{\infty} \mathrm{i}^n c_n \,\mathrm{se}_n(\theta^I, h)\mathrm{se}_n(\theta, h), \tag{25}$$

where $x = (a\cos\theta, b\sin\theta)$ is an evaluation point on the boundary of the cylinder, $h = k^2(a^2 - b^2)/4$ and ce_n, se_n are known as Mathieu functions of the first kind of order n [35]. Coefficients b_n and c_n are dependent upon the boundary conditions. In the hard case, these are obtained from

$$b_n = \frac{\mathrm{Mc}_n^{(1)'}(U,h)\mathrm{Mc}_n^{(3)}(U,h)}{\mathrm{Mc}_n^{(3)'}(U,h)}, \quad c_n = \frac{\mathrm{Ms}_n^{(1)'}(U,h)\mathrm{Ms}_n^{(3)}(U,h)}{\mathrm{Ms}_n^{(3)'}(U,h)},$$

where $U = \mathrm{arctanh}(b/a)$, $\mathrm{Mc}_n^{(1)}, \mathrm{Mc}_n^{(3)}, \mathrm{Ms}_n^{(1)}, \mathrm{Ms}_n^{(3)}$ are modified Mathieu functions [34] and prime denotes differentiation with respect to the first argument. Series (25) converges for $|\cosh U| > 1$ and $\mathrm{Re}\, U > 0$. All Mathieu functions were computed using Special Function FORTRAN Routines available in Ref. [36]. Despite the good accuracy of the functions involved in the series, its evaluation numerically breaks down for $ka > 40$ due to severe roundoff errors when computing coefficients b_n and c_n.

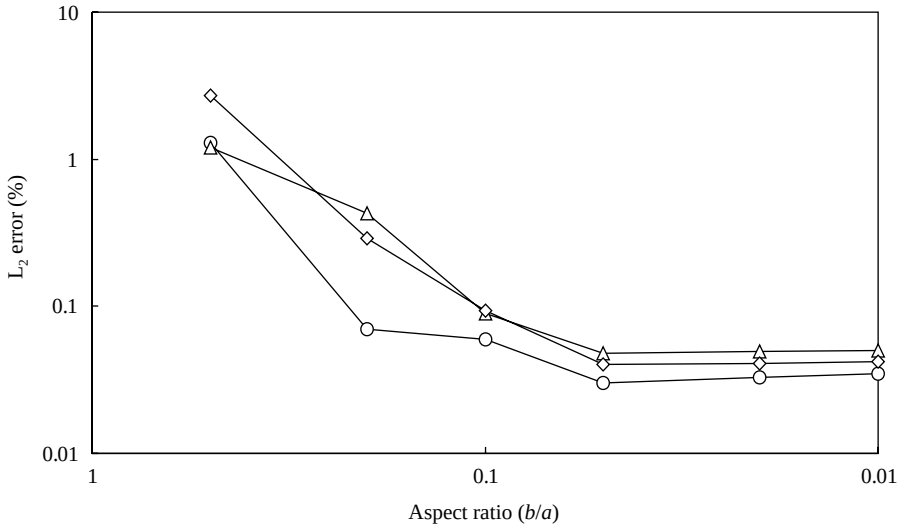

Fig. 3. Error analysis for the hard elliptical cylinder, $ka = 20$. —○—, $\theta^I = 30°$; —△—, $\theta^I = 60°$; —◇—, $\theta^I = 90°$.

The quality of the solution ϕ for a relatively large range of aspect ratios ($0.5 \geqslant b/a \geqslant 0.01$) at $ka = 20$ and three angles of incidence $\theta^I = 30°, 60°$ and $90°$ will be investigated. The elliptical boundary is represented with only *one element* and 24 directions are considered ($N_d = 48$). The L_2 relative errors are displayed in Fig. 3. The decrease of the errors with respect to the aspect ratio is simply due to the increase of the parameter α whose average value is 3.11 at $b/a = 0.5$, 3.75 at $b/a = 0.05$ and 3.76 at $b/a = 0.01$. The strong variations of the errors are then in agreement with results of Fig. 1. The slightly better results obtained when $\theta^I = 30°$ may be attributed to the behaviour of the total potential on the surface of the scatterer that tends to be singular for a vertical incident wave and regular for horizontal incidence.

It should be mentioned that the parameter α is no longer a constant and only its average value $\alpha = N_d\lambda/P$ where P is the perimeter of Γ, is available. For instance, the distance between two samples (i.e., collocation points) located on the flat region of the ellipse ($\theta \sim \pm\pi/2$) is about 1.6 times the average sampling distance. This distortion may affect the quality of the results especially in borderline cases where α is taken to be close to the critical value 2. This sampling problem will no longer be discussed here and this is subject to further investigation.

To visually identify effects of various parameters such as the angle of incidence or boundary conditions, it is convenient to represent the scattered far field on a polar plot. The far field pattern ϕ_∞ is defined by the asymptotic behaviour of the scattered wave $\phi^S(x) = \mathrm{e}^{\mathrm{i}k|x|}|x|^{-1/2}\phi_\infty(\hat{x}) + O(|x|^{-3/2})$ as $|x| \to \infty$, uniformly for all directions $\hat{x} = x/|x|$. From the asymptotics for the Hankel function for large argument and using the fact that $|x - y| = |x| - \hat{x} \cdot y + O(|y|^2/|x|)$, the far field pattern is given by

$$\phi_\infty(\hat{x}) = \sqrt{\frac{k}{8\pi}}\mathrm{e}^{-\mathrm{i}\pi/4} \int_\Gamma (\hat{x} \cdot n(y) + \mathrm{i}v)\mathrm{e}^{-\mathrm{i}k\hat{x}\cdot y}\phi(y)\,\mathrm{d}\Gamma_y. \tag{26}$$

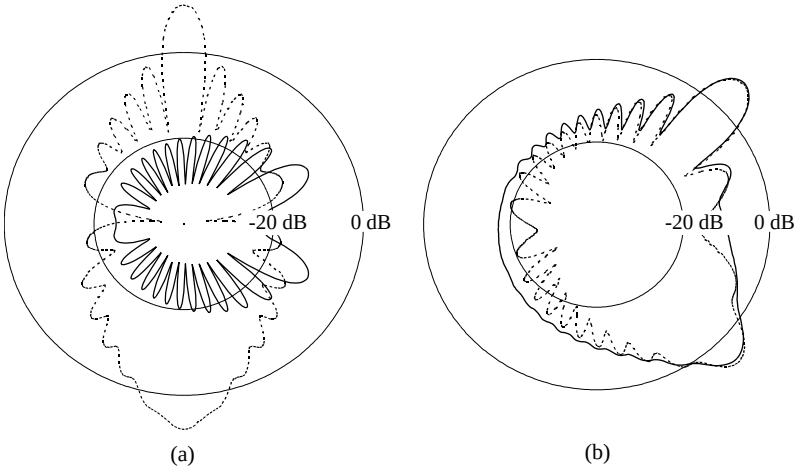

Fig. 4. Far field patterns (dB) for the elliptical cylinder at $ka = 20$ with $b/a = 0.1$. (a) Hard cylinder: straight line, $\theta^I = 0^\circ$; dashed line, $\theta^I = 90^\circ$. (b) Incidence $\theta^I = 45^\circ$: straight line, soft; dashed line, hard.

In Fig. 4(a) far field patterns in decibels (i.e., $10\log_{10}|\phi_\infty|^2$) are shown for two extreme cases $\theta^I = 0^\circ$ and $\theta^I = 90^\circ$ at $ka = 20$ and $b/a = 0.1$. As expected, the scattered field is less intense for horizontal incidence than for vertical. Note that as the aspect ratio tends to zero, the scattered field for $\theta^I = 0^\circ$ will vanish whereas the far field pattern associated with the vertical incidence will be symmetric with respect to the horizontal line. Fig. 4(b) illustrates boundary condition effects for an incidence $\theta^I = 45^\circ$. The soft case has been computed by considering high values for the impedance norm $|v|$ until its effect becomes indistinguishable on the graph. This clearly shows that the scattering in the forward direction is weakly affected by the physical nature of the obstacle while the soft condition strongly attenuates the directivity pattern in the backward direction.

4.2. Multibody wave propagation problems

As a final example, the problem of water wave–structure interaction by an array of four bottom-mounted vertical rigid cylinders of circular section of radius a arranged at the vertices of a square of side length $2b$ is presented. The cylinders, numbered 1–4, are situated at $(-b,-b),(-b,b),(b,b),(-b,b)$, respectively, and extend from the bottom $z = -h$ up through the free surface $z = 0$. This is a typical cylinder configuration with applications in the offshore industry. The reduction of the problem to the Helmholtz equation is accomplished by a separation of variables approach in which the velocity potential $\Phi(x,z,t)$ is taken to have a hyperbolic cosine variation with depth z,

$$\Phi(x,z,t) = -\frac{igH}{2\omega}\frac{\cosh k(z+h)}{\cosh kh}\phi(x)e^{-i\omega t}, \tag{27}$$

where g is the gravitational constant, H is the wave height and ω the wave angular frequency. The wave number k is the real positive solution of the dispersion relation $k\tanh kh = \omega^2/g$. As a

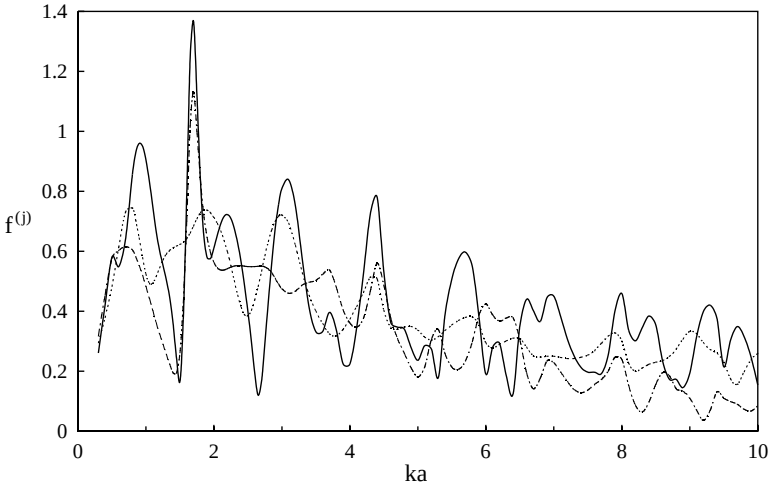

Fig. 5. Non-dimensional amplitude of the first order force in the direction of the wave advance ($b/a = 2$). —cylinder (1), - - - - cylinder (2), – - – - cylinder (3).

practical illustration, consider the first-order hydrodynamic force $F^{(j)}$ exerted on each cylinder due to an incident plane wave $\phi^I(x) = e^{ikd\cdot x}$ with direction $\theta^I = 45^\circ$ so that effects on cylinders 2 and 4 are identical. By denoting $\Gamma^{(j)}$, the boundary line of the horizontal section of the cylinder (j), we have

$$F^{(j)}(t) = -\frac{\rho g H \tanh kh}{2k} e^{-i\omega t} \int_{\Gamma^{(j)}} \phi(y) n(y)\, d\Gamma_y, \tag{28}$$

where ρ is the density of the fluid. In Fig. 5 are displayed the non-dimensional amplitudes

$$f^{(j)} = \frac{1}{2\pi a}\left| \int_{\Gamma^{(j)}} \phi(y)\, d\cdot n(y)\, d\Gamma_y \right| \tag{29}$$

of the first order force in the direction of the wave advance plotted against ka in the case $b/a = 2$. All cylinders are represented with only two elements and $M = 16$ directions were taken. These curves show that multi-body interaction can give rise to important resonance effects on the amplitude of the first order force. These effects can be conveniently illustrated in Fig. 6 where the maximum free-surface elevation amplitude $|\eta| = H/2|\phi|$ (we took $H = 2$) has been plotted at the resonance $ka = 1.7$. The build-up in front of cylinder 3 is over four times the amplitude of the incident wave. For this particular example, the results were checked with the approximate series given in Ref. [37]. In Table 6, the value of the potential at the North pole of each cylinder is compared. Here again, the accuracy is outstanding (8 to 9 exact digits) and the plane wave basis remains very effective in a multi-reflection context.

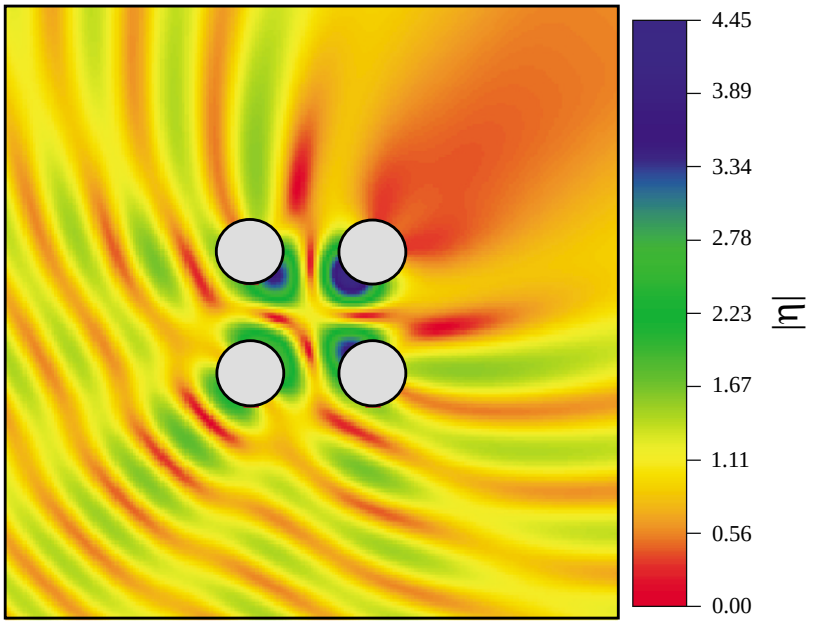

Fig. 6. Maximum free-surface elevation amplitude $|\eta|$ at $ka = 1.7$, $(b/a = 2)$.

Table 6
Comparison with Linton and Evans formula at the North pole of each cylinder at $ka = 1.7$

	ϕ (computed)	$\tilde{\phi}$ (from approximate series in Ref. [37])
Cylinder (1)	$-2.418395682 + i\,0.753719398$	$-2.418395683 + i\,0.753719398$
Cylinder (2)	$2.328927403 - i\,0.310367705$	$2.328927400 - i\,0.310367707$
Cylinder (3)	$0.350611956 - i\,0.198852086$	$0.350611956 - i\,0.198852086$
Cylinder (4)	$-0.383803273 + i\,1.292792457$	$-0.383803272 + i\,1.292792455$

5. Conclusions

This paper has described the use of a plane wave basis to express the potential variable in the Helmholtz problem in a boundary element context. Since the new basis has been included as part of the element shape function, the fundamental solution for this problem remains unchanged, and the new approach may be coded relatively simply.

Accurate results have been demonstrated for classical scattering problems, including cases with multiple cylinders. Some numerical features of the approach have been determined that are essential for its successful usage. These may be summarised as follows: (i) The accurate representation of the geometry of the scattering body. This is a requirement of the physics of the problem, and is not related to the particular technique adopted. When the waves are very short, the results obtained are sensitive to changes in the geometry typically of a tenth of the wavelength. This implies that for relatively long waves, a circular cylinder, for example can be represented as a

high order regular polygon, without any adverse effect upon the results. But for short waves the cylinder must be modelled precisely, if spurious oscillations in the scattered field are to be avoided. Thus the use of standard quadratic shape functions are insufficient in modelling a circular scatterer, because deviations from the precise circle are significant relative to the wavelength. There are implications for the modelling of any short wave scattering object. Its geometry must be known and defined to within a small fraction of the wavelength, if the results are to be relied upon. (ii) The use of a solver that is sympathetic to the poor conditioning that can arise from the plane wave basis. The authors have found success with the singular value decomposition (SVD) algorithm, especially when the system is truncated by eliminating the smallest singular values. A threshold value of $O(10^{-12})$ has been found effective for a variety of cases. (iii) The use of an appropriate number of variables with respect to the frequency. This is commonly defined by the use of about 2.5 degrees of freedom per wavelength, though for problems with more severe distortion between parametric space and real space this number may need to be higher.

In practical terms, the results of this work show that, for any given amount of computational resource, the plane wave basis boundary elements enable the supported frequency range to be extended by a factor of 3–4 over conventional, direct collocation boundary elements for two-dimensional cases. The method may be expected to show even greater improvements in frequency range for three-dimensional analysis. Since this addresses the single most important factor limiting the use of discrete numerical methods in analysis of wave problems, this advance is expected to have a significant impact on a wide variety of engineering simulations.

Acknowledgements

This work has been funded by the EPSRC, under grant GR/N09879. The authors are very grateful to EPSRC for this support for Dr. Emmanuel Perrey-Debain. Peter Bettess is also grateful to the EPSRC Senior Research Fellowship committee, chaired by Professor Sir Richard Brook, which is funding this work, through EPSRC Grant Number: SF/000169. The authors are grateful to BAE SYSTEMS and particularly Dr. David Rowse and Dr. Simon Benham for their support and interest. The authors are also grateful to Dr. Omar Laghrouche and Rie Sugimoto for useful discussions.

References

[1] O.C. Zienkiewicz, R.L. Taylor, The Finite Element Method, Vols. 1–3, Butterworth Heinemann, London, 2000.
[2] C.A. Brebbia, J. Dominguez, Boundary Elements, An Introductory Course, CMP and McGraw-Hill, Southampton and New York, 1992.
[3] I. Babuška, F. Ihlenburg, T. Stroubolis, S.K. Gangaraj, A posteriori error estimation for finite element solutions of Helmholtz equation—Part I: the quality of local error indicators and estimators, International Journal for Numerical Methods in Engineering 40 (1997) 3443–3462.
[4] I. Babuška, F. Ihlenburg, T. Stroubolis, S.K. Gangaraj, A posteriori error estimation for finite element solutions of Helmholtz equation—Part II: the quality of pollution error, International Journal for Numerical Methods in Engineering 40 (1997) 3883–3900.
[5] P. Bettess, O.C. Zienkiewicz, Diffraction and refraction surface waves using finite and infinite elements, International Journal for Numerical Methods in Engineering 11 (1977) 1271–1290.

[6] P. Bettess, Infinite Elements, Penshaw Press, Sunderland, 1992.
[7] D.S. Burnett, R.L. Holford, An ellipsoidal acoustic infinite element, Computer Methods in Applied Mechanics and Engineering 164 (1998) 49–76.
[8] R.J. Astley, W. Eversman, A note on the utility of a wave envelope approach in finite element duct transmission studies, Journal of Sound and Vibration 76 (1) (1981) 560–595.
[9] R.J. Astley, Wave envelope and infinite elements for acoustical radiation, International Journal for Numerical Methods in Engineering 3 (1983) 507–526.
[10] R.J. Astley, J.G. Macaulay, J.P. Coyette, Mapped wave envelope elements and for acoustical radiation and scattering, Journal of Sound and Vibration 170 (1) (1994) 97–118.
[11] R.J. Astley, Infinite elements for wave problems: a review of current formulations and an assessment of accuracy, International Journal for Numerical Methods in Engineering 49 (7) (2000) 951–976.
[12] E. Chadwick, P. Bettess, O. Laghrouche, Diffraction of short waves modelled using new mapped wave envelope finite and infinite elements, International Journal for Numerical Methods in Engineering 45 (1999) 335–354.
[13] J.M. Melenk, I. Babuška, The partition of unity finite element method. Basic theory and applications, Computer Methods in Applied Mechanics and Engineering 139 (1996) 289–314.
[14] J.M. Melenk, I. Babuška, The partition of unity method, International Journal for Numerical Methods in Engineering 40 (1997) 727–758.
[15] T. Stroubolis, I. Babuška, K. Copps, The design and analysis of the generalised finite element method, Computer Methods in Applied Mechanics and Engineering 181 (2000) 43–69.
[16] O. Laghrouche, P. Bettess, Short wave modelling using special finite elements—towards an adaptive approach, 10th Conference on the Mathematics of Finite Elements and Applications X—MAFELAP, Brunel University, England.
[17] O. Laghrouche, P. Bettess, Short wave modelling using special finite elements, Journal of Computational Acoustics 8 (1) (2000) 189–210.
[18] O. Laghrouche, P. Bettess, R.J. Astley, Modelling of short diffraction wave problems using approximating system of plane waves, International Journal for Numerical Methods in Engineering 54 (2002) 1501–1533.
[19] P. Ortiz, E. Sanchez, An improved partition of unity finite element model for diffraction problems, International Journal for Numerical Methods in Engineering 50 (2000) 2727–2740.
[20] P. Mayer, J. Mendel, The finite ray element method for the Helmholtz equation of scattering: first numerical experiments, UCD/CCM Report 111, 1997.
[21] C. Farhat, I. Harari, L. Franca, The discontinous enrichment method, Report Number CU-CAS-00-20, College of Engineering, University of Colorado, Boulder, USA.
[22] A. de La Bourdonnaye, A microlocal discretization method and its utilization for a scattering problem, Comptes Rendus de l'Academie des Science. Paris. Série I 318 (1994) 385–388.
[23] A. de La Bourdonnaye, Convergence of the approximation of wave functions by oscillatory functions in the high frequency limit, Comptes Rendus de l'Academie des Science. Paris. Série I 318 (1994) 765–768.
[24] E. Perrey-Debain, J. Trevelyan, P. Bettess, New special wave boundary elements for short wave problems, Communications in Numerical Methods in Engineering 18 (4) (2002) 259–268.
[25] E. Darve, The fast multipole method: numerical implementation, Journal of Computational Physics 1608 (2000) 195–240.
[26] O.P. Bruno, L.A. Kunyansky, Surface scattering in three dimensions: an accelerated high-order solver, Proceedings of the Royal Society of London Series A 457 (2001) 1–14.
[27] P. Juhl, A numerical study of the coefficient matrix of the boundary element method near the characteristic frequencies, Journal of Sound, Vibration 175 (1) (1994) 39–50.
[28] S. Amini, M. Kirkup, Solution of Helmholtz equation in the exterior domain by elementary boundary integral methods, Journal of Computational Physics 118 (1995) 208–221.
[29] H.A. Schenck, Improved integral formulation for acoustic radiation problems, Journal of the Acoustical Society of America 44 (1968) 41–58.
[30] J.C.F. Telles, A self-adaptive co-ordinate transformation for efficient numerical evaluation of general boundary element integrals, International Journal for Numerical Methods in Engineering 24 (1987) 959–973.

[31] P. Juhl, A note on the convergence of the direct collocation boundary element method, Journal of Sound and Vibration 212 (4) (1998) 703–719.
[32] W.H. Press, A.A. Teukolsky, W.T. Vetterling, B.P. Flannery, Numerical Recipes in Fortran, Cambridge University Press, Cambrdige, 1992.
[33] G.H. Golub, C.F. Van Loan, Matrix Computations, The Johns Hopkins University Press, Baltimore, MD, 1983.
[34] D.S. Jones, Acoustic and Electromagnetic Waves, Clarendon Press, Oxford, 1986.
[35] M. Abramovitz, I. A. Stegun, Handbook of Mathematical Functions, 10th Edition, Applicable Mathematics Series, Vol. 55, National Bureau of Standards, US Government Printing Office, Washington, DC, 1972.
[36] S. Zhang, J. Jianming, Computation of special functions. Available at http://iris-lee3.ece.uiuc.edu/~jjin/specfunc.html.
[37] C.M. Linton, D.V. Evans, The interaction of waves with arrays of vertical circular cylinders, Journal of Fluid Mechanics 215 (1990) 549–569.